Journal of Power Sources 196 (2011) 10538–10542

Contents lists available at SciVerse ScienceDirect

Journal of Power Sources

journal homepage: www.elsevier.com/locate/jpowsour

Precise modification of the interface between titanium dioxide and electrolyte of dye-sensitized solar cells with oxides deposited by thermal evaporation of metals and subsequent oxidation

Chin Yong Neo, Jianyong Ouyang*

Department of Material Science and Engineering, National University of Singapore, Singapore 117574, Singapore

ARTICLE INFO

Article history:
Received 11 July 2011
Received in revised form 12 August 2011
Accepted 12 August 2011
Available online 24 August 2011

Keywords:
Dye-sensitized solar cell
Interface
Alumina
Magnesia
Charge recombination
Thermal evaporation

ABSTRACT

This manuscript reports the modification of the interface between the mesoporous TiO_2 work electrode and electrolyte of dye-sensitized solar cells (DSCs) with oxide layers deposited by the thermal evaporation of metals and subsequent oxidation with UV ozone. Both Al_2O_3 and MgO can be deposited on mesoporous TiO_2 by this method, and their thickness can be precisely controlled. A thin layer of Al_2O_3 or MgO on the TiO_2 work electrode can improve the photovoltaic efficiency. The optimal thicknesses are 14.1 and 4.9 Å for Al_2O_3 and MgO, respectively. The oxide effect has been investigated by the electrochemical impedance spectroscopy, cyclic voltammetry and UV–Vis–NIR absorption spectroscopy. The improvement in the photovoltaic efficiency by an oxide layer is attributed to the upward shift of the conduction band of TiO_2, the passivation of the TiO_2 surface, and the retardation of the charge recombination through the interface between TiO_2 and electrolyte.

1. Introduction

Dye-sensitized solar cells (DSCs) have attracted strong attention since their discovery about twenty years ago [1–5]. They are promising to be the next-generation solar cells because of their low fabrication cost and relatively good photon-to-current conversion efficiency (PCE). PCE as high as about 12% had been reported [6]. A DSC is a photoelectrochemical cell which consists of a mesoporous TiO_2 work electrode, a monolayer of dye chemically anchored to TiO_2, an electrolyte comprising redox species, and a catalytic counter electrode. The work principle of DSCs involves the following steps: (1) Light absorption by the dye and formation of excitons; (2) electron injection from the excited dye molecules into TiO_2; (3) electron transport along the mesoporous TiO_2 electrode; (4) regeneration of dye by the redox species and transport of the redox species from the work electrode to the counter electrode; (5) regeneration of the redox species at the counter electrode. The interface between the TiO_2 work electrode and the electrolyte plays a key role in the photon-to-electricity conversion [7–9]. Electrons are injected from the excited dye molecules through this interface into TiO_2. But charge recombination may take place through this interface as well. The electrons injected into the mesoporous TiO_2 may pass through this interface and recombine with either the oxidized dye molecules or redox species in the electrolyte. The latter is particularly critical for the photovoltaic performance. The charge recombination lowers both the short-circuit current density (J_{sc}) and open-circuit voltage (V_{oc}) [10–14]. It has been demonstrated that the charge recombination can be retarded by coating a thin layer of oxide like Al_2O_3 or MgO with a wide band gap on the mesoporous TiO_2 work electrode [15–30]. This thin insulating oxide layer serves as an energy barrier, which can suppress both the charge recombination and the electron injection. Thus, it is important to precisely control the thickness of this oxide layer so that the charge recombination can be effectively blocked while it does not significantly affect the electron injection from the dye molecules into TiO_2 [31]. Several methods have been reported to fabricate a thin oxide layer on the mesoporous TiO_2 layer. A wet chemical process like the sol–gel process can convert a metal precursor into metal oxide on TiO_2 [17–20]. But it usually requires a sintering step at 450–500 °C to achieve good quality and is thus not suitable for plastic-based flexible DSCs. In addition, the wet chemical process cannot precisely control the thickness of the oxide layer. The thickness can only be varied at a resolution down to 1 nm. Atomic layer deposition (ALD) can precisely deposit a thin oxide layer through a chemical reaction of a metal precursor and has also been used to coat various oxides on TiO_2 of DSCs [24,26–30]. However, as ALD is a chemical technique, there is always a risk of contaminations from the unused precursors [32,33]. Vapor deposition techniques, including

* Corresponding author. Tel.: +65 6516 1472.
E-mail address: mseoj@nus.edu.sg (J. Ouyang).

0378-7753/$ – see front matter © 2011 Elsevier B.V. All rights reserved.
doi:10.1016/j.jpowsour.2011.08.061

magnetron sputtering [25] and chemical vapor deposition [32], were also used to deposit an oxide layer on mesoporous TiO_2. Special equipments are required for ALD and the vapor deposition.

In this manuscript, we report the deposition of oxides on the mesoporous TiO_2 through the thermal evaporation of metals and subsequent oxidization of the metals into oxides. The thickness of the oxide layer can be precisely controlled by this method. Both Al_2O_3 and MgO were coated on TiO_2 by this method. They can remarkably improve the photovoltaic performance of DSCs.

2. Experimental

2.1. Materials

DSL 18 NR-T (20 nm) and WER2-O (350–450 nm) TiO_2 pastes were purchased from Dyesol. Ti-Nanoxide T (20 nm) TiO_2 paste, ruthenium 535-bis TBA, N719 dye, Surlyn (SX1170-250), which are ionomer films of 25 μm thick, were obtained from Solaronix SA. 1-Methyl-3-propylimidazolium iodide (PMII) (purity > 98%), 1-methyl-3-butylimidazolium tetrafluoroborate ($BMIBF_4$) (purity > 97%), 4-tier-butylpyridine (TBP) (purity = 99%), anhydrous tert-butanol (purity > 99.5%), chloroplatinic acid hexahydrate ($H_2PtCl_6{\cdot}6H_2O$), iodine, acetonitrile, aluminium wire (99%) and magnesium ribbons (99.95%) were supplied by Sigma–Aldrich. Valeronitrile and guanidinium thiocynate were got from Fluka. Titanium tetrachloride ($TiCl_4$) was obtained from Merck. All chemicals were used as received.

2.2. Fabrication of DSC

DSCs were fabricated through the conventional process [34]. The TiO_2 work electrode consists of a mesoporous TiO_2 layer of 15 μm in thickness (Dyesol DSL 18NR-T of 10) and a scattering TiO_2 layer of 5 μm in thickness (Dyesol WER4-O Reflector paste). Al was deposited onto the TiO_2 work electrode by thermal evaporation in a vacuum of 1.5×10^{-4} Pa with an Edwards Auto 306 thermal evaporator. The thickness was recorded with an Inficon quartz crystal thickness monitor. Al was converted into Al_2O_3 through the oxidation with a Jelight UV Ozone cleaner 42 for 10 s. MgO was coated onto the TiO_2 layer through a similar process. The TiO_2 electrodes coated with Al_2O_3 or MgO were then immersed in a 0.5 mM N719 dye solution in a cosolvent of acetonitrile/tert-butanol (volume ratio: 1:1) for 24 h. A cell was made by assembling a dye-impregnated TiO_2 electrode with a counter electrode and sealed with a 25 μm-thick Solaronix polymer melt. The counter electrode was fabricated by the pyrolysis of an ethanol solution of 0.2 M H_2PtCl_6 at 400 °C on a fluorine doped tin oxide (FTO) glass for 15 min. The cells were filled with a liquid electrolyte comprising 0.6 M 1-methyl-3-propylimidazolium iodine, 0.03 M I_2, 0.1 M guanidine thiocynate, and 0.5 M 4-tert-butyl pyridine in a cosolvent of acetonitrile/valeronitrile (volume ratio = 85:15).

2.3. Characterization of DSCs

The thicknesses of the TiO_2 layers were determined using a Tencor P-10 Alpha-Step profiler. The absorption spectra were obtained with a Shimadzu UV-1800 UV Spectrophotometer. The X-ray photoelectron spectra (XPS) were acquired using an Axis Ultra DLD X-ray photoelectron spectrometer equipped with an Al Ka X-ray source (1486.6 eV).

The photovoltaic performance of the DSCs was measured with a computer-programmed Keithley 2400 source/meter under AM1.5G Newport's Oriel class A solar simulator (100 mW cm^{-2}), which was certified by the JIS C 8912 standard. A circular mask with a diameter of 5.2 mm was placed on each DSC during the tests. Electrochemical impedance spectra (EIS) and cyclic voltammograms (CV) of the cells were taken with an ECO CHEMIE Autolab (PGSTAT 302N and FRA2). The frequency range of EIS was from 0.1 up to 10^5 Hz, and an ac voltage of 10 mV was superimposed on a dc bias that was set at the V_{oc} of each cell. The CVs were studied in an ionic liquid, 1-methyl-3-butylimidazolium tetrafluoroborate ($BMIBF_4$), with Ag/Ag^+ and Pt as the reference and counter electrode, respectively. The work electrodes were bare mesoporous TiO_2 films or mesoporous TiO_2 films coated with Al_2O_3. The scan rate was 50 mV s^{-1}.

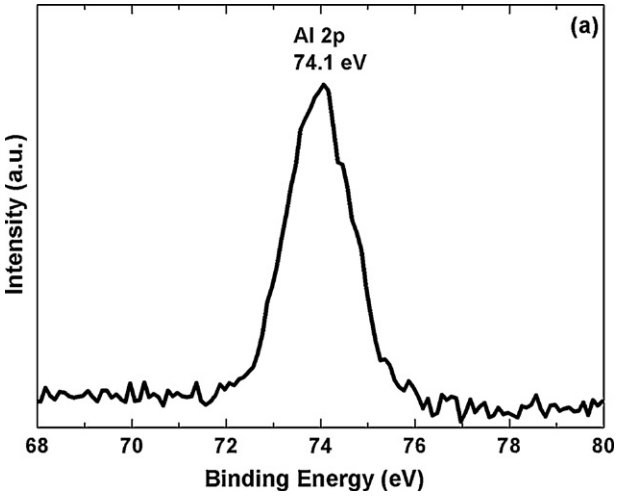

Fig. 1. XPS spectra of Al 2p core level of Al_2O_3 coated on mesoporous TiO_2.

3. Results and discussions

3.1. Improvement in the photovoltaic performance of DSCs by Al_2O_3 and MgO

Al can be readily deposited on TiO_2 through thermal evaporation, and its thickness can be well controlled. After the UV ozone treatment, it was studied by XPS (Fig. 1). The Al 2p XPS band appears at 74.1 eV, and no XPS band corresponding to metallic Al can be observed. The XPS indicates the presence of Al_2O_3 on TiO_2 and the complete conversion of Al into Al_2O_3 after the UV ozone treatment [35]. The thickness of the Al_2O_3 layer can be calculated in terms of the thickness of Al recorded by the thickness monitor during the thermal evaporation, the atomic masses of Al (27 g mol^{-1}) and O (16 g mol^{-1}), and the densities of Al (2.7 g cm^{-3}) and Al_2O_3 (4.0 g cm^{-3}).

The SEM images of a bare mesoporous TiO_2 and a mesoporous TiO_2 coated with a 14.1 Å-thick Al_2O_3 layer (TiO_2/Al_2O_3 (14.1 Å)) are presented in Fig. 2. The thin Al_2O_3 layer does not remarkably affect the mesoporous structure of the TiO_2 work electrode. Thus, it may not affect the penetration of dye molecules and the redox species into the pores.

DSCs with Al_2O_3 layers of various thicknesses were fabricated and characterized. The current density (J)–voltage (V) curves were recorded for DSCs under simulated AM1.5G illumination (Fig. 3). The thickness of the Al_2O_3 layer on the mesoporous TiO_2 electrode was varied from 6.4 up to 25.6 Å. But only the J–V curve for the DSC with an Al_2O_3 layer of 14.1 Å thick is presented for clarity. J–V curve of a control DSC without Al_2O_3 is also presented for comparison. The photovoltaic performances, including J_{sc}, V_{oc}, fill factor (FF) and PCE, are summarized in Table 1. The photovoltaic performances of DSCs, whose J–V curves are not shown in Fig. 3, are also listed in Table 1. The photovoltaic performance of DSCs is sensitive to the thickness of the Al_2O_3 layer. A thin Al_2O_3 layer increases both the V_{oc} and J_{sc} values. The photovoltaic performance is quite sensitive to the thickness of the Al_2O_3 layer. The

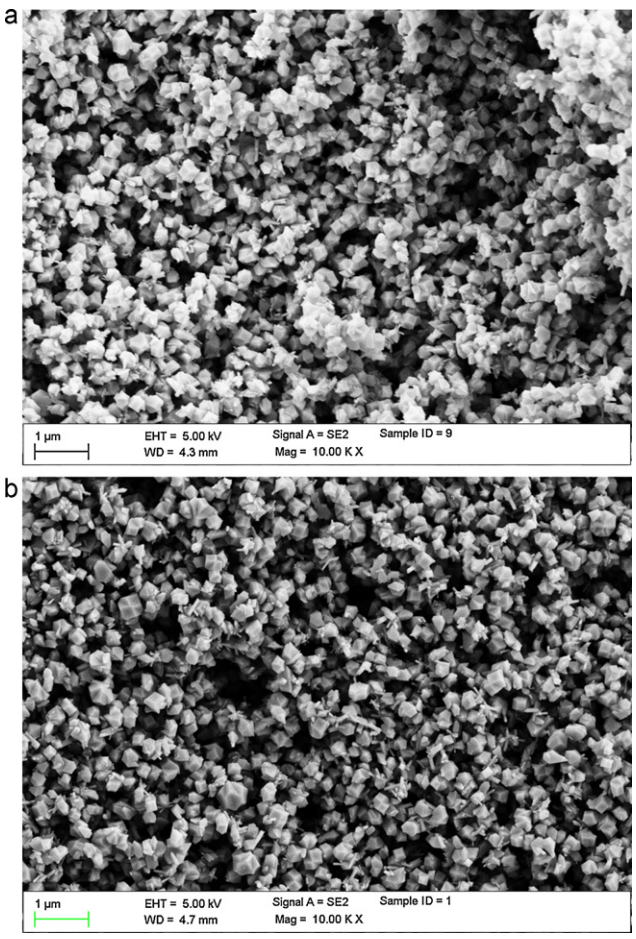

Fig. 2. SEM images of mesoporous TiO_2 coated (a) without and (b) with a 14.1 Å-thick Al_2O_3 layer.

optimal thickness is 14.1 Å. This optimal thickness is comparable to that by ALD [24,27]. The photovoltaic performances at this optimal Al_2O_3 thickness are: V_{oc} = 0.78, J_{sc} = 13.74 mA cm^{-2}, FF = 0.74, and PCE = 7.96%. PCE is remarkably higher than that (7.44%) of the control DSC without the Al_2O_3 layer. In addition, the maximum output power density of the DSC under simulated AM1.5G illumination increased from 7.44 mW cm^{-2} to 7.96 mW cm^{-2} after the modification of the TiO_2 with a 14.1 Å-thick Al_2O_3 layer. Both the V_{oc} and J_{sc} values decrease with the further increase in the thickness of the Al_2O_3 layer. V_{oc}, J_{sc}, PCE and the maximum output power density decrease to 0.75 V, 12.92 mA cm^{-2}, 7.39% and 7.39 mW cm^{-2}, respectively, when the Al_2O_3 layer is 25.6 Å thick.

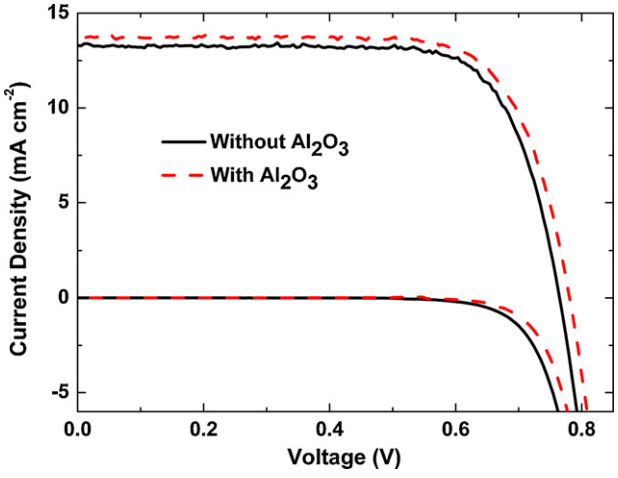

Fig. 3. *J–V* curves of DSCs with the TiO_2 work electrode without (solid curves) and with (dash curves) a 14.1 Å-thick Al_2O_3 layer. The devices were tested under AM1.5 G illumination and in dark.

Table 1
Photovoltaic performances of DSCs with Al_2O_3 layers of various thicknesses.

Thickness of Al_2O_3 (Å)	V_{oc} (V)	J_{sc} (mA cm^{-2})	FF	PCE (%)
0	0.76	12.89	0.76	7.44
6.4	0.78	13.12	0.75	7.70
10.2	0.79	13.25	0.74	7.76
11.5	0.79	13.46	0.74	7.82
12.8	0.79	13.48	0.74	7.87
14.1	0.78	13.74	0.74	7.96
15.4	0.78	13.60	0.75	7.94
19.2	0.76	13.12	0.76	7.56
25.6	0.75	12.92	0.76	7.39

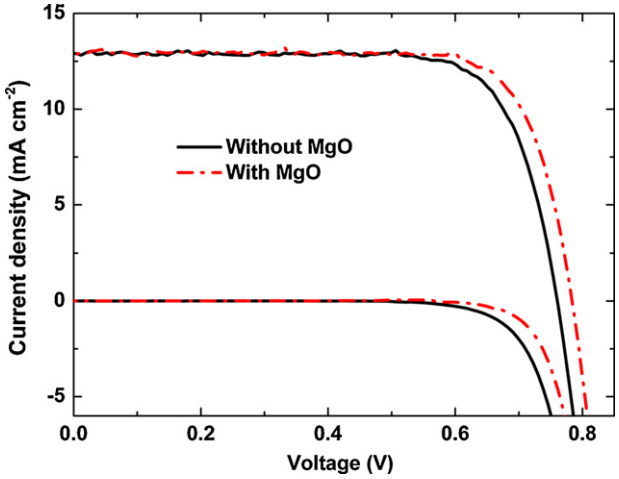

Fig. 4. *J–V* curves of DSCs with the TiO_2 work electrode without (solid curves) and with (dash curves) a 4.9 Å-thick MgO layer. These devices were tested under AM1.5G illumination and in dark.

Depositing an insulating oxide layer on the TiO_2 work electrode has been reported for DSCs in literature. It is somewhat strange that relative poor PCEs ranging from 3.7% to 5.75% were usually reported for the control DSCs without the insulating oxide layer. Although remarkable improvement in the PCE was observed after the deposition of an insulating oxide layer, the PCEs of the modified DSCs were still in the range from 5% to 6.5%. It is important to improve the performance of high-performance control devices. In this research work, the deposition of an Al_2O_3 layer can improve the PCE from 7.44% to 7.96%. The PCE of the modified DSCs is higher than most of the PCE values reported for modified DSCs in literature.

Besides Al_2O_3, MgO was also coated on the mesoporous TiO_2 electrodes through the thermal deposition of Mg and subsequent oxidation by UV ozone. The photovoltaic *J–V* curves of DSCs with MgO are presented in Fig. 4, and the photovoltaic performances are summarized in Table 2. These results indicate that the optimal thickness of the MgO layer is 4.9 Å. The photovoltaic performance

Table 2
Photovoltaic performances of DSCs with MgO layers of various thicknesses.

Thickness of MgO (Å)	V_{oc} (V)	J_{sc} (mA cm^{-2})	FF	PCE (%)
0	0.76	12.89	0.76	7.44
4.1	0.77	13.14	0.76	7.76
4.9	0.78	12.95	0.77	7.82
5.7	0.76	13.19	0.76	7.63
8.1	0.78	13.00	0.77	7.77
12.2	0.78	12.78	0.77	7.66

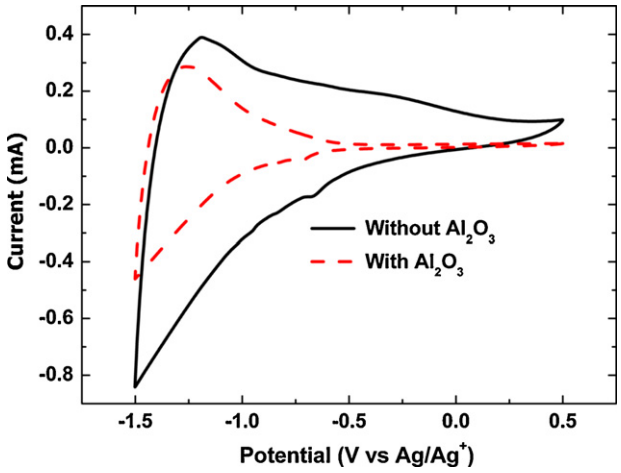

Fig. 5. Cyclic-voltammograms of TiO_2 (solid line) and TiO_2 coated with a 14.1 Å-thick Al_2O_3 layer (dashed line).

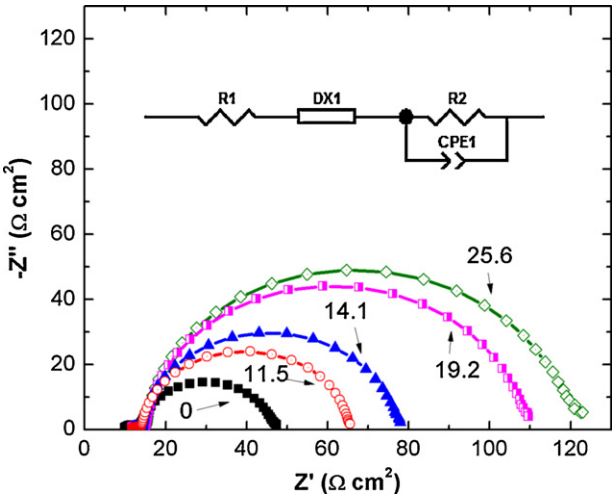

Fig. 6. Nyquist plots of DSCs with a 0, 11.5, 14.1, 19.2 and 25.6 Å-thick Al_2O_3 layer coated on the TiO_2 work electrode. The inset is the equivalent circuit.

at the optimal thickness is: V_{oc} = 0.78, J_{sc} = 12.95 mA cm^{-2}, FF = 0.77, and PCE = 7.82%. Accordingly, the maximum output power density increases from 7.44 mW cm^{-2} to 7.82 mW cm^{-2}. The photovoltaic performance slightly decreases when the MgO layer becomes thicker.

3.2. Mechanism for Al_2O_3-induced improvement in photovoltaic performance of DSCs

The oxide effect on the photovoltaic performance of DSCs was investigated by CV, EIS and UV–Vis–NIR absorption spectroscopy. TiO_2 and TiO_2/Al_2O_3 were used as the work electrode for CV (Fig. 5). In principle, for a junction between an n-type semiconductor like TiO_2 and electrolyte, electron injection will commence once the quasi-Fermi level of the electrolyte reaches the lowest edge of the conduction band of the semiconductor. The CV can be affected by the presence of coordinatively unsaturated Ti species on the surface of TiO_2 which causes the existence of electronic levels at energies below the conduction band edge [36–38]. These surface states give rise to the graduate onset capacitance current as observed on the CV of the bare mesoporous TiO_2. The current increases much more slowly for the TiO_2/Al_2O_3 electrode than that for the bare TiO_2 electrode during the potential scan from 0.5 to −1.5 V versus Ag/Ag^+. This indicates the surface passivation of TiO_2 by Al_2O_3 [39]. The onset anodic current shifts to a more negative potential for the TiO_2/Al_2O_3 electrode, in comparison to the bare TiO_2 electrode. This indicates that Al_2O_3 shifts the conduction band of TiO_2 upward [23,38]. The oxide-induced shift in the conduction band of TiO_2 was also observed by other techniques [39,40]. The passivation of the TiO_2 surface can reduce the dark current, and the upward shift of the conduction band contributes to the increase in V_{oc} of the DSCs with an Al_2O_3 layer.

The oxide effect is also studied by EIS. Nyquist plots of DSCs with a bare mesoporous TiO_2 and a mesoporous TiO_2/Al_2O_3 work electrodes were extracted from the EIS data (Fig. 6). There are usually two or three arcs or semicircles in the Nyquist plot of a DSC. The first semicircle at the high frequency range is attributed to the charge transfer at the counter electrode [41–43]. The second semicircle at the middle frequency range is due to the charge transfer at the TiO_2/electrolyte interface and the electron transport through the mesoporous TiO_2 work electrode. The first process for the charge transfer through the TiO_2/electrolyte interface is the main contribution for the impedance in this frequency range [44,45]. The third arc in the low-frequency range originates from the Nernstian diffusion of the redox species through the electrolyte. The big semicircles in the Nyquist plots in Fig. 6 correspond to the charge transfer at the TiO_2/electrolyte interface and the electron transport through the mesoporous TiO_2 work electrode [46].

The resistances (R) corresponding to the semicircles in the middle frequency range were calculated by fitting the Nyquist plots. They were plotted versus the thickness of the Al_2O_3 layer (Fig. 7). $\ln R$ almost linearly increases with the increasing Al_2O_3 thickness (t), that is, $R \alpha e^{\beta t}$, where β is constant. This relationship is consistent with the charge tunneling mechanism. Thus, the insulating Al_2O_3 layer can reduce the charge recombination.

The UV–Vis absorption spectra of TiO_2 and TiO_2/Al_2O_3 impregnated with the dye molecules were measured to understand possible effect of Al_2O_3 on the dye impregnation (Fig. 8). The two absorption spectra are almost the same. Hence, coating of Al_2O_3 does not affect the dye loading on the work electrode, because the dye molecules can also anchor on the surface of Al_2O_3. This confirms that the Al_2O_3-induced increase in J_{sc} is mainly due to the retardation of the charge recombination.

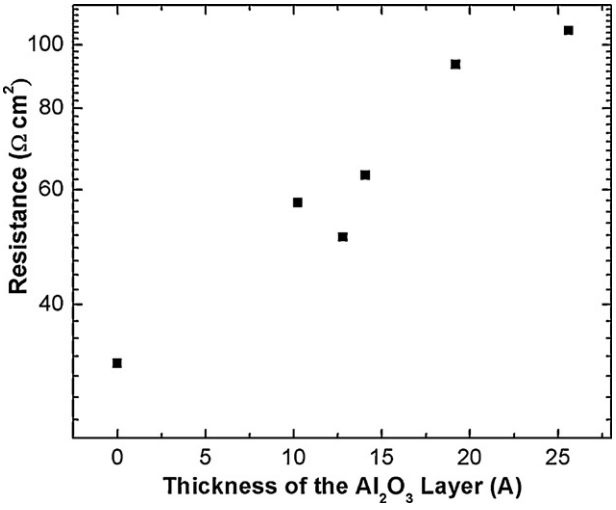

Fig. 7. Variation of the resistance corresponding to the second arc of ac impedance spectrum with the thickness of the Al_2O_3 layer coated on the mesoporous TiO_2 work electrode of DSCs.

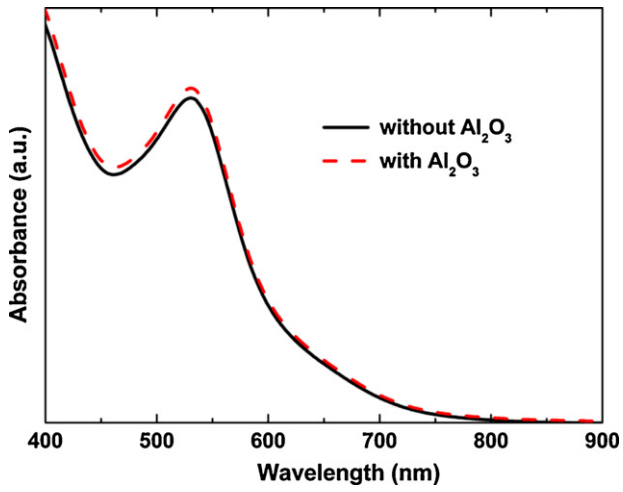

Fig. 8. UV–Vis absorption spectra of dye-impregnated TiO_2 without and with a 14.1 Å-thick Al_2O_3 layer coated on the TiO_2 layer.

4. Conclusions

In conclusion, metal oxides with precise thickness can be coated on mesoporous TiO_2 through the thermal evaporation of the corresponding metals and subsequent oxidation with UV-ozone. Both Al_2O_3 and MgO are coated on the mesoporous TiO_2 electrodes by this method. An oxide layer can remarkably improve the photovoltaic performance of DSCs. The photovoltaic performance is sensitive to the thickness of the oxide layer. The optimal thicknesses are 14.1 and 4.9 Å for Al_2O_3 and MgO, respectively. The oxide effect on the photovoltaic performance of DSCs is attributed to the passivation of the TiO_2 surface, upward shift of the conduction band of TiO_2, and retardation of the charge combination.

Acknowledgement

This research work was financially supported by a research grant from the Ministry of Education, Singapore (Project No. R-284-000-080-112).

References

[1] B. Oregan, M. Grätzel, Nature 353 (1991) 737–740.
[2] M. Grätzel, J. Photochem. Photobiol. C: Photochem. Rev. 4 (2003) 145–153.
[3] M. Grätzel, Nature 414 (2001) 338–344.
[4] P. Joshi, Y. Xie, M. Ropp, D. Galipeau, S. Beiley, Q. Qiao, Energy Environ. Sci. 2 (2009) 426–429.
[5] T. Xu, Q. Chen, D.H. Lin, H.Y. Wu, C.F. Lin, Q. Qiao, J. Photon. Energy 1 (2011) 011107.
[6] K. Kalyanasundaram, Dye-Sensitized Solar Cells, EPFL Press, Lausanne, 2010.
[7] A. Stanley, D. Matthews, Aust. J. Chem. 48 (1995) 1293–1300.
[8] Y. Ogomi, T. Kato, S. Hayase, J. Photopolym. Sci. Technol. 19 (2006) 403–408.
[9] X. Feng, K. Shankar, M. Paulose, C.A. Grimes, Angew. Chem. Int. Ed. 48 (2009) 8095–8098.
[10] J.R. Durrant, S.A. Haque, E. Palomares, Coord. Chem. Rev. 248 (2004) 1247–1257.
[11] M.D. Archer, A.J. Nozik, Nanostructured and Photoelectrochemical Systems for Solar Photon Conversion, Imperial College Press, London, 2008.
[12] R. Argazzi, C.A. Bignozzi, T.A. Heimer, F.N. Castellano, G.J. Meyer, J. Am. Chem. Soc. 117 (1995) 11815–11816.
[13] P. Bonhote, J.E. Moser, R. Humphrey-Baker, N. Vlachopoulos, S.M. Zakeeruddin, L. Walder, M. Grätzel, J. Am. Chem. Soc. 121 (1999) 1324–1336.
[14] G.D. Sharma, P. Suresh, M.S. Roy, J.A. Mikroyannidis, J. Power Sources 195 (2010) 3011–3016.
[15] Y. Diamant, S.G. Chen, O. Melamed, A. Zaban, J. Phys. Chem. B 107 (2003) 1977–1981.
[16] S.G. Chen, S. Chappel, Y. Diamant, A. Zaban, Chem. Mater. 13 (2001) 4629–4634.
[17] A. Zaban, S.G. Chen, S. Chappel, B.A. Gregg, Chem. Commun. 223 (2000) 1–2232.
[18] J. Xia, N. Masaki, K. Jiang, S. Yanagida, Chem. Commun. 13 (2007) 8–140.
[19] E. Palomares, J.N. Clifford, S.A. Haque, T. Lutz, J.R. Durrant, Chem. Commun. 146 (2002) 4–1465.
[20] E. Palomares, J.N. Clifford, S.A. Haque, T. Lutz, J.R. Durrant, J. Am. Chem. Soc. 125 (2003) 475–482.
[21] B.C. O' Regan, S. Scully, A.C. Mayer, E. Palomares, J.R. Durrant, J. Phys. Chem. B 109 (2005) 4616–4623.
[22] Z. Liu, K. Pan, M. Liu, M. Wang, Q. Lu, J. Li, Y. Bai, T. Li, Electrochim. Acta 50 (2005) 2583–2589.
[23] V. Ganapathy, B. Karunagarani, S.W. Rhee, J. Power Sources 195 (2010) 5138–5143.
[24] C. Lin, F.Y. Tsai, M.H. Lee, C.H. Lee, T.C. Tien, L.P. Wang, S.Y. Tsai, J. Mater. Chem. 19 (2009) 2999–3003.
[25] S. Wu, H. Han, Q. Tai, J. Zhang, S. Xu, C. Zhou, Y. Yang, H. Hu, B.L. Chen, X.Z. Zhao, J. Power Sources 182 (2008) 119–123.
[26] T.W. Hamann, O.K. Farha, J.T. Hupp, J. Phys. Chem. C 112 (2008) 19756–19764.
[27] C. Prasittichai, J.T. Hupp, J. Phys. Chem. Lett. 1 (2010) 1611–1615.
[28] M. Shanmugam, M.F. Baroughi, D. Galipeau, Thin Solid Films 518 (2010) 2678–2682.
[29] T.C. Tien, F.M. Pan, L.P. Wang, C.H. Lee, Y.L. Tung, S.Y. Tsai, C. Lin, F.Y. Tsai, S.J. Chen, Nanotechnology 20 (2009) 305201.
[30] M. Nanu, J. Schoonman, A. Goossens, Adv. Mater. 16 (2004) 453–456.
[31] V. Makinen, K. Honkala, H. Hakkinen, J. Phys. Chem. C 115 (2011) 9250–9259.
[32] M. Leskel, M. Ritala, Angew. Chem. Int. Ed. 42 (2003) 5548–5554.
[33] T.O. Kääriäinen, P. Maydannik, D.C. Cameron, K. Lahtinen, P. Johansson, J. Kuusipalo, Thin Solid Films 519 (2011) 3146–3154.
[34] S. Ito, P. Chen, P. Comte, M.K. Nazeeruddin, P. Liska, P. Pechy, M. Grätzel, Prog. Photovolt. Res. Appl. 15 (2007) 603–612.
[35] H. Zhang, J. Ouyang, Appl. Phys. Lett. 97 (2010) 063509.
[36] J. Moser, S. Punchihewa, P.P. Infelta, M. Gratzel, Langmuir 7 (1991) 3012–3018.
[37] A. Halfeldt, M. Gratzel, Chem. Rev. 95 (1995) 49–68.
[38] Z.P. Zhang, S.M. Zakeeruddin, B.C. O'Regan, R. Humphry-Baker, M. Gratzel, J. Phys. Chem. B 109 (2005) 21818–21824.
[39] G. Zheng, J. Wang, X. Liu, A. Yang, H. Song, Y. Guo, H. Wei, C. Jiao, S. Yang, Q. Zhu, Z. Wang, Appl. Surf. Sci. 256 (2010) 7327–7330.
[40] J. Bandara, U.W. Pradeep, Thin Solid Films 517 (2010) 952–956.
[41] X. Mei, S.J. Cho, B. Fan, J. Ouyang, Nanotechnology 21 (2010) 395202.
[42] K. Sun, B. Fan, J. Ouyang, J. Phys. Chem. C 114 (2010) 4237–4244.
[43] B. Fan, X. Mei, K. Sun, J. Ouyang, Appl. Phys. Lett. 93 (2008) 143103.
[44] J. Bisquert, J. Phys. Chem. B 106 (2002) 325–333.
[45] M. Adachi, M. Sakamoto, J. Jiu, Y. Ogata, S. Isoda, J. Phys. Chem. B 110 (2006) 13872–13880.
[46] Q. Wang, S. Ito, M. Grätzel, F. Fabregat-Santiago, I. Mora-seró, J. Bisquert, T. Bessho, H. Imai, J. Phy. Chem. B 110 (2006) 25210–25221.